Proceedings of the 19th Lunar and Planetary Science Conference, pp. 433-441

Phase Diagram for Ammonia-Water Mixtures at High Pressures: Implications for Icy Satellites

H. C. Cynn

Department of Earth and Space Sciences, University of California, Los Angeles, CA 90024-1567

S. Boone, A. Koumvakalis, and M. Nicol

Department of Chemistry and Biochemistry, University of California, Los Angeles, CA 90024-1569

D. J. Stevenson

Division of Geological and Planetary Sciences, California Institute of Technology, Pasadena, CA 91125

The $(NH_3)_X(H_2O)_{1-X}$ phase diagram for $0 \leq X \leq 0.50$ has been reexamined at temperatures from 125 K to 400 K and at pressures to 6.0 GPa using diamond-anvil cells. By electroplating the gasket materials with gold, complicated reactions between sample solutions and gasket materials, which affected earlier studies, have been avoided. Sample pressures were determined using the ruby-luminescence technique, and phase assignments were made using optical characterization. Phase assignments were confirmed by Raman spectroscopy. At room temperature the stable phases observed were fluid, high pressure ices (VI and VII), and ammonia monohydrate, $NH_3 \cdot H_2O$. The Ice VI and Ice VII liquidi at 295 K were extrapolated to intersect at $X = 0.26 \pm 0.01$ and 2.1 GPa. At room temperature, the eutectic for Ice VII and $NH_3 \cdot H_2O$ was observed at 3.3 ± 0.2 GPa, and extrapolation of the room temperature liquidus indicates that the cotectic composition is near $X = 0.45$. Near $X = 0.33$, the stable phases were high pressure ices (VI, VII, and VIII), $NH_3 \cdot H_2O$, and another phase tentatively identified as ammonia dihydrate, $NH_3 \cdot 2H_2O$. At this composition, the Ice VI liquidus and the congruent melting curve of $NH_3 \cdot 2H_2O$ interesect at 1.8 ± 0.2 GPa and 252 ± 5 K, and the Ice VII liquidus is approximately linear with a slope of 0.016 ± 0.002 GPa K^{-1}. To within the uncertainty of the experiment, the Ice VI liquidus continues smoothly from the Ice VII liquidus. The quadruple point among $NH_3 \cdot H_2O$, $NH_3 \cdot H_2O$, Ice VI, and fluid is located at 250 ± 5 K and 1.9 ± 0.3 GPa, with the accompanying double cotectic at a composition of $X = 0.36 \pm 0.01$. The eutectic for $NH_3 \cdot H_2O$ and Ice VII is approximately linear with a slope of 0.033 ± 0.003 GPa K^{-1}. We have applied these data to the interior of Titan in a manner similar to the analysis of Lunine and Stevenson (1987). The main implication of these results is that Titan is likely to have a thicker $NH_3 \cdot H_2O$ ocean than previously suspected, because the stability field of $NH_3 \cdot 2H_2O$ is smaller than previously supposed. Implications for methane and ammonia volcanism on Titan are briefly discussed. The experimentally observed reactivity between the liquid and iron (for example) may also have implications for planetary and satellite evolution.

INTRODUCTION

Primordial ices constitute a large fraction of the material from which the planets and satellites formed. Because few data exist on the properties of these composites at high pressure, models of the structures, dynamics, and histories of the cellestial bodies in the outer solar system have been based on extrapolation of atmospheric pressure data for the relevant mixtures and high pressure data for the pure compounds. The research reported here was conceived as a starting point for a larger study of the high-pressure properties of mixtures of importance to planetary physics. This particular binary system was studied because it was expected to be the simplest to prepare, and because the results could be effectively applied to modeling the structures of the larger icy satellites of the outer solar system, especially Titan. These bodies are large enough to require consideration of high pressure morphology, but small enough that they did not accumulate the light gases, helium and hydrogen (*Lunine and Stevenson*, 1985).

The phase relationships of the ammonia-water system at ambient presure in the liquidus region were investigated early in this century by *Postma* (1920), *Elliott* (1924), and others using optical observations of crystallization and melting. At that time, two stoichiometric compounds were identified: ammonia hemihydrate, $2NH_3 \cdot H_2O$, and ammonia monohydrate, $NH_3 \cdot H_2O$ (M). In older literature, these compounds are referred to as ammonium oxide and ammonium hydroxide, respectively. Using differential scanning calorimetry, *Rollet and Vuillard* (1956) reported the discovery of a third compound, ammonia dihydrate, $NH_3 \cdot 2H_2O$ (D), which had evidently failed to form or had gone unnoticed during earlier studies, presumably because of metastability. The crystal structures of both ammonia monohydrate and ammonia hemihydrate have been investigated using single crystal X-ray diffraction by *Siemons and Templeton* (1954) and *Olovsson and Templeton* (1959), respectively, and the IR spectra of these compounds and their isotopic analogs have been reported by *Bertie and Morrison* (1980, 1981) and by *Bertie and Shehata* (1985). *Bertie and Shehata* (1984) also collected the powder X-ray diffraction pattern and IR spectra of ammonia dihydrate and used these data to deduce a crystal structure. *Hildenbrand and Giauque* (1953) investigated the thermal properties of the monohydrate and the hemihydrate; *Chan and Giauque* (1964) performed a similar study of the dihydrate. According to these workers, none of the hydrates form solid solutions, and none appear to

have residual third law entropied as a result of disordered hydrogen bonding. Relevant density data for these compounds and the fluid are reviewed by *Croft et al.* (1988).

The high-pressure phase diagram of pure water, which constitutes an end member to the binary system in question, has been investigated from the earliest days of high-pressure research. For details, the reader is referred to *Mishima and Endo* (1980) and references therein. Subsequent papers deal with this subject, but those report on temperature and pressure ranges that are not directly relevant to the present inquiry. The melting curve of the monohydrate was reported by *Johnson et al.* (1985) for pressures from 0 GPa to 6.0 GPa. Extensive investigation of the Raman spectra of the monohydrate by A. Koumvakalis (in preparation) at pressures from 0 GPa to 13.5 GPa and at temperatures from 120 K to 450 K give no indication of additional polymorphs.

In a recent report from this laboratory, *Johnson and Nicol* (1987) described parts of the ammonia-water phase diagram and their implications for icy satellites. This report was based on experimental observations of $(NH_3)_X(H_2O)_{1-X}$ mixtures for $0 \leq X \leq 0.34$ in diamond-anvil cells at pressures from 0 GPa to 5.0 GPa and at temperatures from 240 K to 370 K. When an attempt was made to extend the study to higher ammonia concentrations, some observations were very inconsistent with the results in the report just cited. Later, evidence of reaction between the caustic samples and the gasket materials was repeatedly observed. The melting curve for the dihydrate, extrapolated from data in *Johnson and Nicol* (1987), is also difficult to reconcile with thermal data (*Chan and Giauque,* 1964) and density data for the liquid (*Croft et al.,* 1988) and for the solid (*Bertie and Shehata,* 1984). This inconsistency was acknowledged as a potential problem by *Johnson and Nicol* (1987), who speculated on the possibility of a low-lying phase transition for the compound. This is discussed in some detail by *Lunine and Stevenson* (1987) and by *Croft et al.* (1988). When an attempt was made to confirm the identification of the solid assumed to be dihydrate using X-ray diffraction, the crystal structure was inconsistent with the low-pressure crystal structure of the dihydrate, as determined by *Bertie and Shehata* (1984), but corresponded well to that of Ice VI, as reported by *Kamb* (1965). These results prompted a reexamination of the system using gasket materials that are more inert and alternate analytical methods.

EXPERIMENTAL

Samples were compressed in diamond-anvil cells based on two designs: one developed by *Hirsch and Holzapfel* (1981) intended for Raman spectroscopy and another by *Merrill and Bassett* (1974) intended for X-ray diffraction. The beryllium seats on the Merrill-Bassett cells were replaced by stainless steel ones. Pressures in the sample were determined by the ruby-luminescence technique (*Piermarini et al.,* 1975). The pressure and temperature dependences were assumed to be additive, and the temperature correction was based on a calibration performed by *Yen* (1986) in this laboratory. Although such calibrations are known to vary between ruby samples, ours is in good agreement with that reported by *Buchsbaum et al.* (1984). Gaskets were prepared from Inconel 718, stainless steel 301, or work-hardened stainless steel 316 and were electroplated with gold according to a procedure outlined by *Parker* (1963).

Samples with composition $X \leq 0.30$ were prepared by volumetric dilution of commercially available solutions (Fisher Scientific ammonium hydroxide, 28-30% NH_3, catalog no. A669-500) with distilled water. Compositions of the solution were determined by titration with standard hydrochloric acid using bromcresol green as indicator. Samples in this composition range were loaded by immersing the open diamond-anvil cell in the cold solution and closing it. Compositions of the solutions were checked after loading and after extended storage. Samples with compositions $X > 0.30$ were formulated gravimetrically from anhydrous ammonia (Air Products, 99.99%) and vacuum-degassed, distilled water mixed in closed

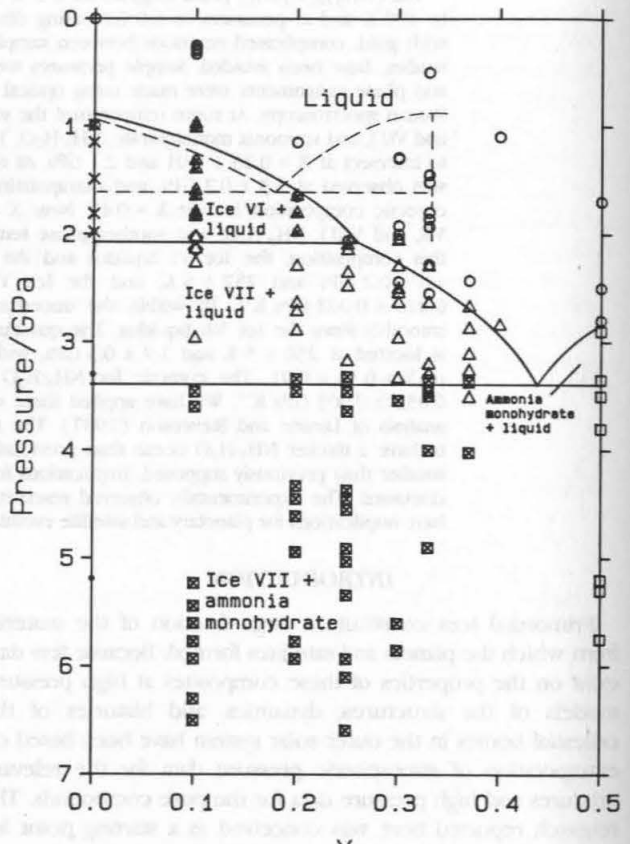

Fig. 1. Compositions, pressures, and phase assignments for $(NH_3)_X(H_2O)_{1-X}$ mixtures at 293 ± 3 K, and the isothermal phase diagram for the water-rich region derived from those data. Symbols represent individual data: circle, liquid; cross, Ice VI; dot, Ice VII; triangle, Ice VII + liquid; box, ammonia monohydrate; triangle with cross, Ice VI + liquid; box with cross, monohydrate + Ice VII. solid lines are phase boundaries assigned from these data. Dashed lines are phase boundaries reported by *Johnson and Nicol* (1987). The precision of the pressure measurement is approximately 0.2 GPa.

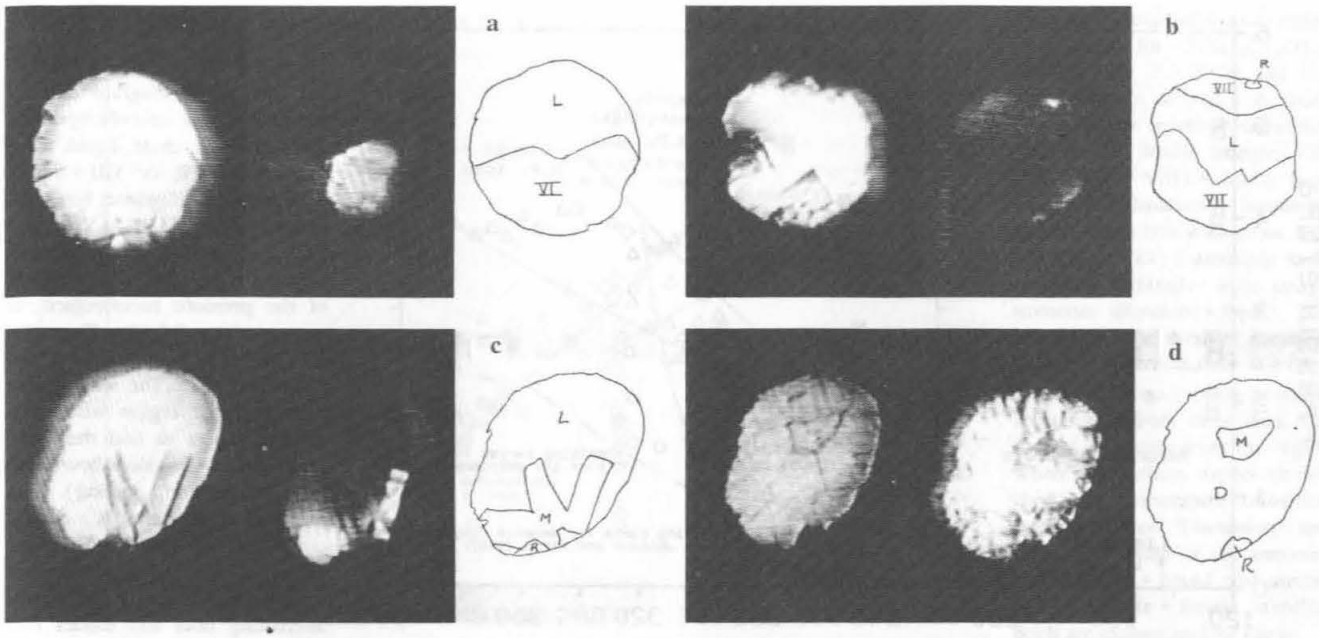

Fig. 2. Visual images of samples of ammonia-water mixtures under high pressure in diamond cells. The left image in each pair is the sample under transmitted lighting; the right image is the same sample between crossed polarizers. The sketches show the phase assignments: L, liquid; M, ammonia monhydrate; D, ammonia dihydrate; VI, Ice VI; VII, Ice VII; R, ruby. Compositions and conditions are as follows: **(a)** X = 0.200, T = 291 K, P = 1.8 GPa; **(b)** X = 0.300, T = 291 K, P = 2.4 GPa; **(c)** X = 0.370, T = 243 K, P = 2.0 GPa; and **(d)** X = 0.370, T = 199 K, P = 1.7 GPa.

stainless steel containers. Samples in this composition range were loaded by injecting a solution into a closed loading cell, which contained an open diamond-anvil cell under vacuum, and subsequently closing the diamond cell. In order to insure injection, it was necessary to maintain the pressure in the mixing vessel at 0.27 MPa with nitrogen gas. A sample of the excess solution could be collected for analysis in a sample vessel connected to the loading cell. This sample was neutralized with excess standard hydrochloric acid and back-titrated with standard sodium hydroxide, using the same indicator. The titration analysis consistently agreed with the formulation to within 0.3 mol.%.

The sample temperature was controlled by isolating the diamond cell in a vacuum cryostat. The copper block in which the cell was mounted was electrically heated and cooled by circulating refrigerants or by thermal contact with a reservoir filled with cryogenic liquid. The temperature was monitored using copper-constantan thermocouples, which were calibrated against liquid nitrogen, dry ice, a bath containing distilled water and ice, and boiling distilled water. Optical observations were made *in situ* using a stereoscope with an optional television camera. The images shown were recorded on videotape and photographed from the monitor. Polarizing filters could be used to observe and record pleochroism and birefringence.

Raman and ruby emission spectra were collected on a Spex 1/4 m monochromator with a 1200 groove/mm grating. Spectra were detected using a Princeton Instrument IRY 1024/G optical multichannel analyzer and recorded on an IBM PC. This spectrometer has a resolution of about 0.6 Å, which corresponds to an uncertainty of about 0.2 GPa for the ruby pressure determination. Argon ion laser light (wavelengths 4765 and 4880 Å) was used as an excitation source for both the Raman and the ruby emission. Some ruby emission spectra were also collected on a Jarrell-Ash 1/2 m monochromator with a 1200 groove/mm grating and a photomultiplier detector. The spectral resolution of this spectrometer is comparable to that described above.

RESULTS

Figure 1 shows phase identification data for samples at various compositions and pressures at room temperature. Descriptions of observed phases are as follows: the liquid appeared featureless under normal and oblique lighting and displayed maximum extinction between crossed polarizers; at room temperature the ruby could be induced to move if surrounded by liquid; most solids displayed grain boundaries, which were accentuated under oblique lighting; Ice VI formed blocky crystals, which displayed weak birefringence (see Fig. 2a); Ice VII formed similar crystals and displayed extinction equivalent to the liquid (see Fig. 2b); and ammonia monohydrate showed pronounced birefringence (see Fig. 2c) and pleochroism.

Figures 3 and 4 show phase identification data for samples at various pressures and temperatures with compositions near X = 0.333 and at X = 0.370, respectively. Descriptions of the observed phases agreed with those listed above. Ice VIII

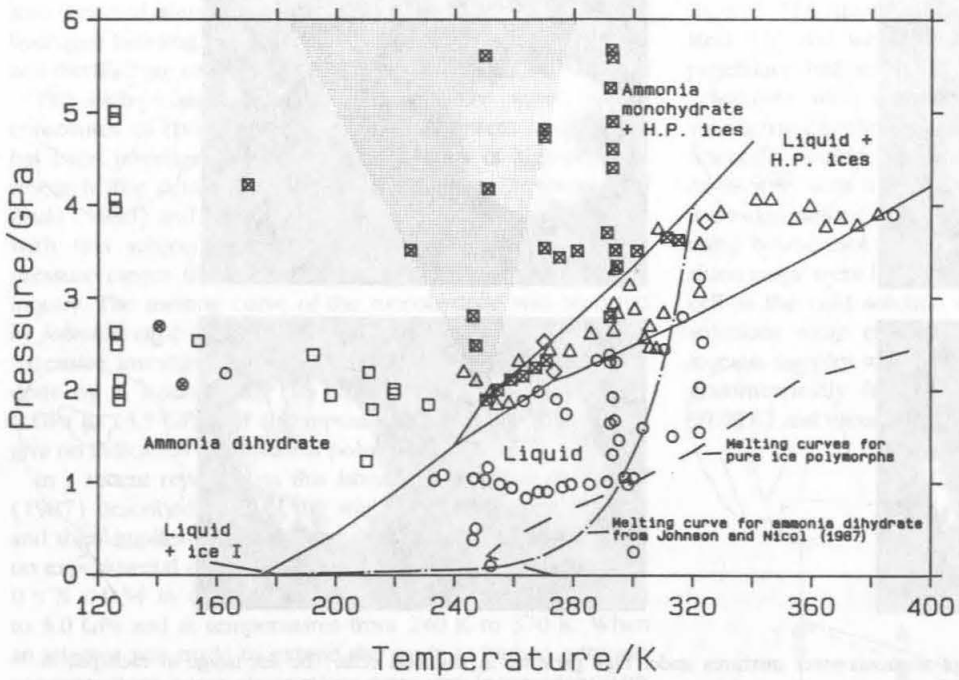

Fig. 3. Conditions and phase assignments for $(NH_3)_X(H_2O)_{1-X}$ mixtures for $X = 0.335 \pm 0.003$ and the phase diagram derived from those data. Symbols represent individual data: circle, liquid; triangle, Ice VI, VII, or VIII + liquid; box, ammonia dihydrate; box with cross, Ices (VI, VII, or VIII) + ammonia monohydrate; circle with cross, glass. The precision of the pressure measurement is approximately 0.2 GPa. The solid lines are phase boundaries assigned from these data. The shaded area represents the region where the authors expect to find the "low-temperature transition boundary" (see "Discussion" section). Also included in the figure is a dashed curve that represents the melting curves of the high-pressure pure ice polymorphs and a curve with alternating dots and dashes that represents the congruent melting curve of the dihydrate proposed by *Johnson and Nicol* (1987).

showed weak birefringence and otherwise resembled Ice VII. Many of the data at low temperature assigned as liquid were probably featureless glass; the glass differed from the liquid only in that it displayed grain boundaries and prevented the ruby from dropping. The formation of a stoichiometric solid at compositions near X = 0.33 was also observed (see Fig. 2d). This solid showed pronounced birefringence between crossed polarizers. Based on its region of stability, its optical properties, and its Raman spectrum (see below), this solid is assumed to be the same dihydrate phase observed by workers listed above. Thus far we have been unable to form this phase from the fluid outside a rather narrow set of conditions: from 1.5 GPa to 2.0 GPa and from 193 K to 208 K. Allowing for a pressure-induced temperature shift, the crystallization region is reasonably consistent with that reported by *van Kasteren* (1973), although van Kasteren's phase transition assignments do not agree with those reported here. (In this work van Kasteren seems to be unaware of the existence of dihydrate. He reports two phase transitions, whose temperatures agree to within about 1 K with those assigned by *Rollet and Vuillard* (1956) to the dihydrate-ice peritectic and the metastable monohydrate-ice eutectic. He assigns these transitions to eutectics between monohydrate and Ice I_h and between monohydrate and Ice I_c, although he fails to specify clearly which is which.) The apparent gap in the crystallization region between 1.5 GPa and ambient pressure could be attributed to lack of patience on the part of the experimenter.

Figure 5 shows representative Raman spectra for various samples. These are intended to confirm phase identifications only; analyses of these spectra will be included in future publications. The new phase consistently showed a spectral fingerprint different from the phases formed at higher pressures and temperatures (i.e., monohydrate and ices). Since the monohydrate and dihydrate have similar optical properties, it is difficult to distinguish between these phases using optical observations alone. The weakness of the symmetric stretch mode of water (~3100 cm^{-1}) in the spectra of these samples (see Fig. 5a) is compelling evidence that the observed substance is a distinct phase. If the phase we describe were actually monohydrate, a considerable amount of high-pressure ice would have been present, which would produce a strong symmetric stretch peak (see Figs. 5b,c).

DISCUSSION

Because our recent findings are in conflict with previously reported results, it is appropriate to discuss the differences in experimental technique between the two investigations. There are four principal differences between the techniques used by *Johnson and Nicol* (1987) and those used here: loading procedure, gasket materials, optical elements, and the use of alternate methods to confirm phase assignments. The reasons for and implications of the first three alterations in procedure will be covered in the order given; there is little need to discuss the fourth.

For most samples with compositions of $X \leq 0.31$, *Johnson and Nicol* (1987) loaded the cell by placing a drop of the cold standardized solution directly on the gasket hole and quickly closing the cell. Subsequent comparison tests between this technique and immersion loading (using gold-electroplated gaskets for both) indicate that, even when performed extremely rapidly, use of the "eye dropper" loading method results in a depletion in ammonia concentration of approximately 5 mol.% when the stock solution has a composition of 30 mol.% ammonia. Presumably, the reason for

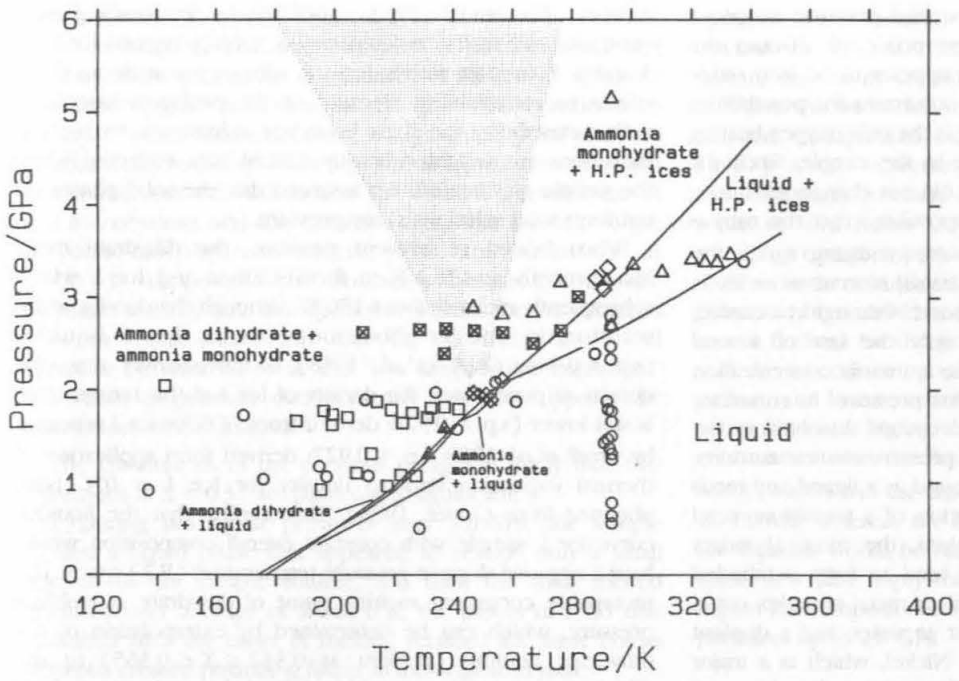

Fig. 4. Conditions and phase assignments for $(NH_3)_X(H_2O)_{1-X}$ mixtures for X = 0.370 and the phase diagram derived from those data. Symbols represent individual data: circle, liquid; triangle, Ices (VI, VII, or VIII) + liquid; box, ammonia dihydrate + ammonia monohydrate; box with cross, Ices (VI, VII, or VIII) + ammonia monohydrate; triangle with cross, ammonia dihydrate + liquid. The precision of the pressure measurement is approximately 0.2 GPa. The solid lines are phase boundaries assigned from these data. The shaded area represents the region where the authors expect to find the "low-temperature transition boundary" (see "Discussion" section). The width of the ammonia monohydrate + liquid and ammonia dihydrate + liquid stability fields are exaggerated for clarity.

the disparity between the two techniques is the large surface-to-volume ratio in a single droplet of solution.

The error associated with the use of the "eye dropper" loading technique does not account for the apparent large depletions of ammonia that would result in the formation of Ice VI in samples with stock compositions $0.25 \leq X < 0.33$. When a brown residue was observed on the surface of the sample hole wall during experiments using stainless steel 316 at high temperatures, the possibility of reaction with other gasket materials and/or the ruby had to be considered. No direct evidence (visible residues, spectroscopic differences, etc.) for reaction of the solution with Inconel 718 has been observed, but the indirect evidence is formidable. A comparison between the room temperature liquidus reported by *Johnson and Nicol* (1987) and the liquidus data reported in this work (see Fig. 1) illustrates this well. It should be stressed that no conclusive method has been devised to analyze the composition of the sample inside the diamond cell; we have had to rely on the repeatability of diagnostic phase transitions to assess whether the sample composition had changed over time. Whenever there was a doubt, data collected between the suspect observation and the previous high temperature run were discarded. Consequently, the majority of the data reported here are taken from fresh samples no more than a few days old.

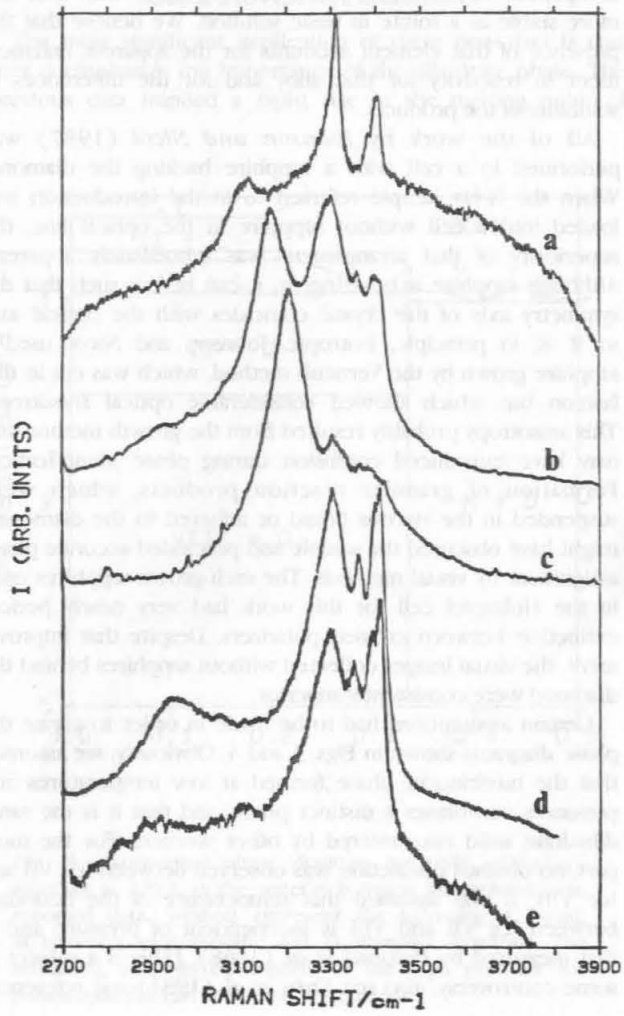

Fig. 5. Raman spectra for samples of $(NH_3)_X(H_2O)_{1-X}$ at high pressures. Sample compositions, conditions, and phase assignments are as follows: **(a)** X = 0.333, T = 127 K, P = 2.1 GPa, ammonia dihydrate; **(b)** X = 0.200, T = 295 K, P = 5.9 GPa, ammonia monohydrate + Ice VII; **(c)** X = 0.0, T = 295 K, P = 5.2 GPa, Ice VII; **(d)** X = 0.50, T = 295 K, P = 5.2 GPa, ammonia monohydrate; and **(e)** X = 0.50, T = 160 K, P = 8.2 GPa, ammonia monohydrate.

Although the mechanisms of the high-pressure reactions observed are unknown, it is appropriate to discuss the possibilities. The formation of what appears to be iron oxide on the surface of the stainless steel constrains the possibilities dramatically. Besides the ruby, water is the only oxygen-bearing compound of significant abundance in the sample. Since the luminescence spectrum of the ruby did not change with time, it is unlikely (although far from impossible) that the ruby is the source of oxygen. If water is the oxidizing agent, the reduced hydrogen must dissolve in the solution or more likely diffuse through the metal or the diamond. Although reasonable, this process probably represents only the last of several reactions; alone it would increase the ammonia concentration and cause an increase in the liquidus pressure. Intermediate reactions could well produce metal cations dissolved in the solution along with hydroxyl ions to preserve electroneutrality. Ammonia is typically more tightly bound as a ligand and tends to displace water during the formation of a transition metal complex. Iron, nickel, and chromium, the most abundant components of the alloys used, all tend to form octahedral complexes. Thus formation of a trivalent metal complex could deplete ammonia up to twice as fast as water, and a divalent complex up to three times as fast. Nickel, which is a major component of Inconel, is more easily oxidized than iron and more stable as a solute in basic solution. We believe that the presence of that element accounts for the apparent enhancement in reactivity for that alloy and for the differences in solubility of the products.

All of the work by *Johnson and Nicol* (1987) was performed in a cell with a sapphire backing the diamond. When the X-ray sample referred to in the introduction was loaded into a cell without sapphire in the optical line, the superiority of that arrangement was immediately apparent. Although sapphire is birefringent, it can be cut such that the symmetry axis of the crystal coincides with the optical axis so it is, in principle, isotropic. Johnson and Nicol used a sapphire grown by the Verneuil method, which was cut in this fashion but which showed considerable optical anisotropy. This anisotropy probably resulted from the growth method and may have introduced confusion during phase identification. Formation of granular reaction products, which were suspended in the viscous liquid or adhered to the diamonds, might have obscured the sample and precluded accurate phase assignment by visual methods. The melt-grown sapphires used in the Holzapfel cell for this work had very nearly perfect extinction between crossed polarizers. Despite that improvement, the visual images collected without sapphires behind the diamond were consistently superior.

Certain assumptions had to be made in order to create the phase diagrams shown in Figs. 3 and 4. Obviously, we assumed that the birefringent phase formed at low temperatures and pressures constitutes a distinct phase, and that it is the same dihydrate solid encountered by other workers. For the most part, no obvious distinction was observed between Ice VII and Ice VIII. It was assumed that temperature of the boundary between Ice VII and VIII is independent of pressure and is that measured by *Pistorius et al.* (1968). [This is a subject of some controversy; also see *Kuhs et al.* (1984) and references therein.] The reader may be confused by apparently glaring contradictions in the assignments of stability regions for Figs. 3 and 4. Like most authors on the subject, we attribute these effects to metastability. Because of the problems associated with metastability, the phase boundary assignments for melting transitions are weighted heavily toward data collected when the sample was heated. We assumed that the solid phases do not form solid solutions at any pressure.

When heated at ambient pressure, the dihydrate melts incongruently at 176.1 K to form solution and Ice I, which subsequently melts at about 180 K. Although the density of the solution in the neighborhood of the Ice I liquidus (s.p. = 0.946; *Croft et al.,* 1988) is much lower than the density of pure water, the density of Ice I at this temperature is still lower (s.p. = 0.928; derived from EOS for Ice I reported by *Croft et al,* 1988; s.p. = 0.927; derived form application of thermal expansion data to density for Ice I at 0°C both obtained from *Clarke,* 1928). This implies that the liquidus curve for a sample with constant overall composition would have a negative slope in pressure-temperature (P-T) space. The metastable congruent melting point of dihydrate at ambient pressure, which can be determined by extrapolation of the dihydrate liquidus (present at $0.342 \leq X \leq 0.365$) to the dihydrate composition, is within 1 K of the peritectic melting point. This transition was actually observed at 176.16 ± 0.05 K by *Chan and Giauque* (1964). It is unlikely that ammonia dihydrate is one of those rare substances with a negative change of volume of fusion (in this pressure regime, a metastable transition), and unless the shape of the dihydrate liquidus changes radically with increasing pressure, the peritectic boundary is constrained to parallel the metastable melting curve quite closely. Thus the peritectic boundary should have a positive P-T slope. Therefore the temperature difference between the peritectic and the Ice I liquidus should rapidly decrease with increasing pressure. Because the temperature difference between them is small at ambient pressure, less than 0.2 GPa, these transitions should meet to form the congruent melting curve of the dihydrate. Since the P-T slope for the ambient pressure Ice I liquidus is negative, it is not unnatural to assume that the ice liquidi retain roughly the same shape as the melting curves of the various pure ice polymorphs at all compositions. This last assumption has important consequences. If the melting data from Fig. 4 are used to estimate the shape of the congruent melting curve of the dihydrate, and the melting curves for the pure ices (see Fig. 3) are used to estimate the general shape of liquidi for the ices at $X = 0.333$, the two curves will cross twice: once at low pressure where the congruent melting curve of dihydrate emerges, as discussed above, and again at around 2.0 GPa. The second crossing would correspond to the onset of a high-pressure peritectic and Ice VI liquidus completely analogous to the situation at ambient pressure. Because of the difference between the P-T slopes of the melting curve of dihydrate and the Ice VI liquidus, these boundaries would be expected to diverge as the pressure increases. As these transitions diverge in P-T space, the intersection of the Ice VI liquidus and the dihydrate liquidus in temperature-composition space must move to higher values of X. As the pressure rises,

this intersection would eventually encounter the cotectic between dihydrate and monohydrate. The point at which this occurs corresponds to the coincidence of the Ice VI, dihydrate and monohydrate solubility curves, and thus constitutes a "tritectic" point. Since that point is a quadruple point and thus invariant, this transition must separate at higher pressures into two transitions: the formation of the eutectic between Ice VI and monohydrate and the transition from that eutectic to the dihydrate-monohydrate eutectic. The latter transition at $X = 0.333$ represents the boundary between the pure dihydrate stability field and the stability fields for the eutectics between monohydrate and Ices VI, VII, and VIII. It will hereafter be referred to as the "low-temperature transition." The room-temperature data presently reported supports the conclusions of this analysis.

The conclusions of the previous paragraph imply that two transitions at $X = 0.37$ are particularly significant:

1. During heating at pressures near 1.0 GPa, the sample formed a liquid phase that appeared to occupy only a small fraction of the sample volume, and then the solid melted gradually over a range of about 6 K; the pieces of solid that remained after the onset of melting retained the same colors between crossed polarizing filters as the original crystal.

2. When the sample was heated at pressures near 1.8 GPa, the melting was abrupt. The liquid phase filled at least 2/3 of the sample volume, and the small crystals that remained bore no obvious resemblance to the original solid phase; these crystals were very birefringent, so it is unlikely that they were Ice VI.

These transitions were assigned as the pseudocongruent melting of dihydrate (the liquidus is probably very close to the solidus at this composition) and the melting of the dihydrate-monohydrate eutectic leaving the monohydrate, respectively. The presence of a monohydrate-liquid stability field at this pressure and composition indicates that the tritectic point must lie at a composition $0.33 < X < 0.37$, probably closer to $X = 0.37$. The fact that both transitions are observed indicates that the conditions for the eutectic must lie between the conditions for these transitions. Thus the tritectic point must lie at a pressure higher than 1.6 GPa and at a temperature higher than 245 K. A reasonable extension of the liquidus for Ice VII intersects the extrapolation of the eutectic for Ice VII and monohydrate at about 2.1 GPa and 255 K, which forms an upper bound for the tritectic point for temperature and pressure.

The low-temperature transition boundary is constrained to temperatures lower than the metastable extension of the congruent melting curve of dihydrate. Unfortunately, this tells us very little, and the fact that the triple point for Ices VI, VII, and VIII is nearby only complicates matters. If the tritectic is below the boundary between Ices VI and VIII, as it crosses that boundary, the low-temperature transition boundary would have a kink, which would send it toward lower temperatures. The data shown in Fig. 3 suggest that the boundary should intersect the y-axis at approximately 5.2 GPa ($dP/dT = -0.026$ GPa/K), but the data from Fig. 4 suggest that the boundary should be at even lower temperatures, which is not consistent with the low-temperature data in Fig. 3. In the opinions of the the authors, the effects of metastability are so obvious in this data and so well documented by other researchers that no conclusion should be drawn at this time.

Within the water-rich region, the melting curve for ammonia dihydate extrapolated from the data of *Johnson and Nicol* (1967) would constrain the attainable composition of an ammonia-water solution in equilibrium with the appropriate solids to well below 20 mol.% ammonia (see Fig. 1 as an example) except at pressures less than 0.2 GPa. Figures 6 and 7 show isothermal phase diagrams interpolated from the data presented here and from the results of other investigators. Our recent findings for the pure ammonia-water system appear to shift the eutectic composition of the solution to near 30 mol.% ammonia at low temperatures (see Fig. 6) and to even high compositions at higher temperatures (see Figs. 1 and 7). The contrast between the liquidus data reported by *Johnson and Nicol* (1985) and the data presented here can be summarized as follows: Whereas the older data indicate that the shape of the liquidus would be radically altered at fairly low pressures, these new data imply that the general shape of the liquidus region for compositions $0 \leq X \leq 0.50$ is roughly the same for pressures up to 2.0 GPa.

SOLAR SYSTEM APPLICATIONS

The most significant implication of these new data is that they deemphasize the importance of the dihydrate phase. The previous data implied a rapid rise in the melting point of

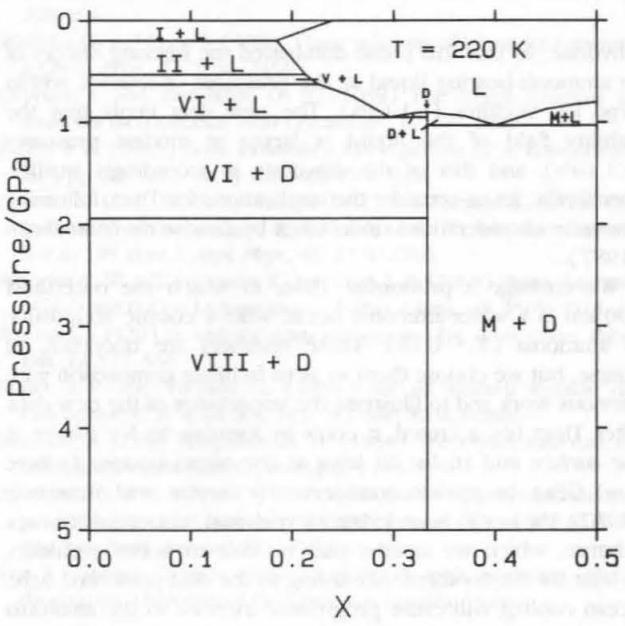

Fig. 6. Isothermal phase diagram for $(NH_3)_X(H_2O)_{1-X}$ mixtures at 220 K in the water-rich region interpolated from reported data. Symbols represent the following: L, liquid; M, ammonia monohydrate; and D, ammonia dihydrate. The remaining symbols correspond to the high pressure ice polymorphs that carry the same designations.

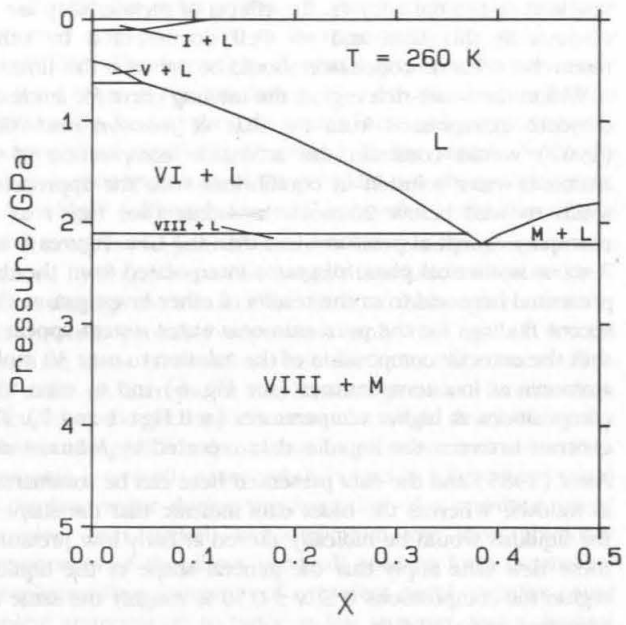

Fig. 7. Isothermal phase diagram for $(NH_3)_X(H_2O)_{1-X}$ mixtures at 260 K in the water-rich region interpolated from reported data. Symbols represent the following: L, liquid, and M, ammonia monohydrate. The remaining symbols correspond to the high-pressure ice polymorphs that carry the same designation.

dihydrate, so that this phase dominated the freezing history of an ammonia-bearing liquid at the pressures of interest within large icy satellites (~1 GPa). The new data imply that the stability field of the liquid is larger at modest pressures (<1 GPa), and that of the dihydrate is accordingly smaller. Specifically, let us consider the implications for Titan, following the same considerations undertaken by *Lunine and Stevenson* (1987).

We envisage a primordial Titan, in which the outermost 700 km is a water-ammonia ocean with a cosmic abundance of ammonia (X ~ 0.16). These numbers are uncertain, of course, but we choose them so as to facilitate comparison with previous work and to illustrate the importance of the new data. After Titan has accreted, it cools by forming an Ice I layer at the surface and an Ice VI layer at the ocean bottom (where P ~1 GPa). In models considered by *Lunine and Stevenson* (1987), the ocean is underlain by rock and primordial ice-rock mixture, which we assume play no role in ocean evolution, at least for the moment. According to the data presented here, ocean cooling will cause progressive increase in the ammonia content of the liquid until X ~ 0.3. At this stage, the base of the ocean must be at roughly P ~ 0.6 GPa (by mass balance) and T ~ 205 K (slight extrapolation of the phase boundary data). The only solid phases that have formed are pure water ices (I and VI, possibly IV). This is markedly different from the implications of the previous data, which predicted large accumulations of dihydrate and an accordingly thinner, less ammonia-rich ocean (see Fig. 7, *Lunine and Stevenson,* 1987). Perhaps more importantly, these new data predict a deep ocean that persists down to a very low temperature. At T = 205 K, the overlying Ice I layer has high viscosity and may be only marginally capable of transporting the expected present-day radiogenic heat output of Titan by solidus convection. It is possible that Titan is still hotter than 205 K at P ~ 0.6 GPa, implying that no ammonia-bearing solids have formed in the age of the solar system.

The striking difference between the old and new data implications is illustrated in Fig. 8 where the corresponding implications for ocean thickness are shown. The temperature scale can also be translated into a time scale, as *Lunine and Stevenson* (1987) discuss, but with very large uncertainties because of the poorly known heat flux from below and rheologies of the various ice phases. The implications of a deeper, more ammonia-rich ocean are as follows.

1. The thick ocean almost certainly persists to the present day, overlain by an Ice I layer that is presently ~150 km in thickness. The current ocean thickness is probably 300-400 km.

2. The uppermost part of the ocean is only slightly more dense than the overlying Ice I (*Croft et al.,* 1988), suggesting the possibility of a modest degree of ammonia-water volcanism during Titan's history, should the overlying ice be contaminated with a few percent rock from later impacts.

3. The particular scenario of methane eruption described by *Lunine and Stevenson* (1987) is now less plausible, since it requires that partially soluble methane is fluxed through the

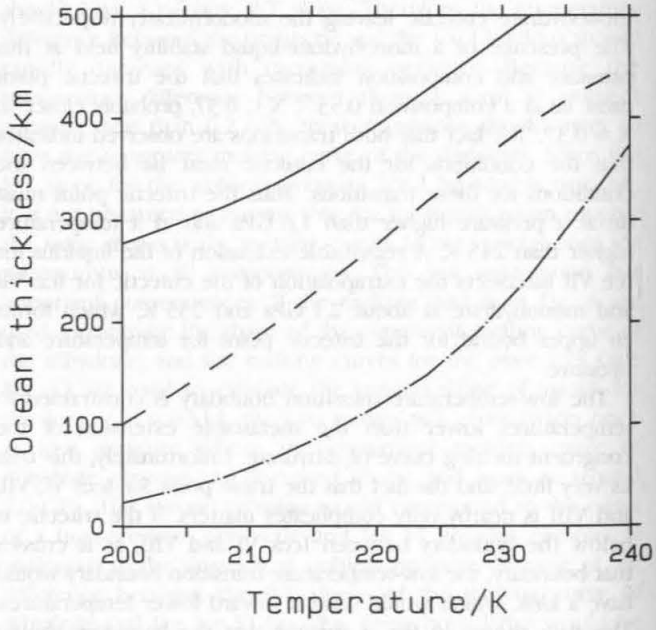

Fig. 8. Ocean thickness as a function of approximate ocean temperature for Titan. Solid line is based on data presented in this paper; dashed and dot-dashed curves are previous estimates from *Lunine and Stevenson* (1987, Fig.7).

ocean from the underlying core, a process that is less likely as the ocean thickens. However, the higher ammonia content of the ocean helps to reduce the stability field of methane clathrate (*Lunine and Stevenson,* 1985), so some methane may still erupt to the surface. Some of these considerations may also apply to Triton.

Finally, we comment on the intriguing possibility that the ammonia-water ocean is chemically reactive at high pressures, forming ion complexes and modifying the oxidation state of cosmically abundant rock-forming species. As a satellite like Titan accretes, rock particles will sediment from the water-ammonia ocean, undergoing solution reactions to the extent that thermodynamics and surface-limited kinetics allow. It is difficult to estimate the quantitative implications of this, since we do not know the particle size distribution of the rock dust or the extent of reaction. However, some general qualitative expectations are these: (1) The ocean may be expected to contain some fraction of the total radiogenic element reservoir (K, U, and Th primarily); and (2) any volcanism may transport metallic atoms (e.g., Fe) to the surface of Titan, where they may form complexes or residues that affect observable properties (e.g., surfacial appearance, radar reflectivity, and color of the hydrocarbon ocean, if any).

From a broader perspective, the enhanced reactivity at high pressure raises some fascinating questions concerning the interiors of the giant planets. Is it correct to assume that the "rock" and "ice" components are chemically distinct, or do they react to such an extent that the distinction is no longer meaningful? These issues must await future experimental and theoretical efforts.

Acknowledgments. This research was supported by NASA grant NAGW-104 and a NASA Graduate Student Researcher Fellowship (SB). We would like to thank G. Schubert for helpful comments.

REFERENCES

Bertie J. E. and Morrison M. M. (1980) The infrared spectra of the hydrates of ammonia, $NH_3 \cdot H_2O$ and $2NH_3 \cdot H_2O$ at 95°K. *J. Chem. Phys., 73,* 4832-4837.

Bertie J. E. and Morrison M. M. (1981) Infrared spectra of $^{15}NH_3 \cdot H_2O$, $2^{15}NH_3 \cdot H_2O$, and deuterated forms of ammonia hemihydrate at 90°K. *J. Chem. Phys, 74,* 4361-4371.

Bertie J. E. and Shehata M. R. (1984) Ammonia dihydrate: Preparation, X-ray powder diffraction pattern and infrared spectrum of $NH_3 \cdot 2H_2O$ at 100 K. *J. Chem. Phys., 81,* 27-30.

Bertie J. E. and Shehata M. R. (1985) The infrared spectra of $NH_3 \cdot H_2O$ and $ND_3 \cdot D_2O$ at 100 K. *J. Chem. Phys., 83,* 1449-1456.

Buchsbaum S., Mills R. L., and Schiferl D. (1984) Phse diagram of N_2 determined by Raman spectroscopy from 15 to 300 K at pressures to 52 kbar. *J. Phys. Chem., 88,* 2522-2525.

Chan J. P. and Giauque W. F. (1964) The entropy of $NH_3 \cdot 2H_2O$. Heat capacity from 15 to 300°K. *J. Phys. Chem., 68,* 3053-3057.

Clarke J. R. (1928) Density and thermal expansion of chemical compounds in the crystalline state, under atmospheric pressure. In *International Critical Tables, Vol. III* (E. W. Washburn, ed.), pp. 43-45. McGraw-Hill, New York.

Croft S. K., Lunine J. I., and Kargel J. (1988) Equation of state of ammonia water liquid: Derivation and planetological application. *Icarus, 73* 279-293.

Elliot L. D. (1924) The freezing point curve of the system water-ammonia. *J. Phys. Chem., 28,* 887-889.

Johnson M. L. and Nicol M. (1987) The ammonia-water phase diagram and its implications for icy satellites. *J. Geophys. Res., 92,* 6339-6349.

Johnson M. L. Schwake A., and Nicol M. (1985) Partial phase diagram for the system $NH_3 \cdot H_2O$: The water-rich region. In *Ices in the Solar System* (J. Klinger et al., eds.), pp. 39-47. Reidel, Dordrecht, Holland.

Hildebrand D. L. and Giauque W. F. (1953) Ammonium oxide and ammonium hydroxide. Heat capacities and thermodynamic properties from 15 to 300°K. *J. Am. Chem. Soc., 75,* 2811-2818.

Hirsch K. R. and Holzapfel W. B. (1981) Diamond anvil high-pressure cell for Raman spectroscopy. *Rev. Sci. Instrum., 52,* 52-55.

Kamb B. (1965) Structure of ice VI. *Science, 150,* 205-209.

Kuhs W. F., Finney J. L., Vettier C., and Bliss D. V. (1984) Structure and hydrogen ordering in ices VI, VII, and VIII by neutron powder diffraction. *J. Chem. Phys., 81,* 3612-2623.

Lunine J. I. and Stevenson D. J. (1985) Thermodynamics of clathrate hydrate at low and high pressures with applications to the outer solar system. *Astrophys. J. Suppl. Ser., 58,* 493-531.

Lunine J. E. and Stevenson D. J. (1987) Clathrate and ammonia hydrates at high pressure: Application to the origin of methane on Titan. *Icarus, 70,* 61-77.

Merrill L. and Bassett W. A. (1974) Miniature diamond anvil pressure cell for single crystal X-ray diffraction studies. *Rev. Sci. Instrum., 45,* 290-294.

Mishima O. and Endo S. (1980) Phase relations of ice under pressure. *J. Chem. Phys., 73,* 2454-2456.

Olovsson I. and Templeton D. H. (1959) The crystal structure of ammonia monohydrate. *Acta Crystallogr., 12,* 827-832.

Parker E. A. (1963) Gold. In *Modern Electroplating* (F. A. Lowenheim, ed.), pp. 207-277. Wiley and Sons, New York.

Piermarini G. J., Block S., Barnett J. D., and Forman R. A. (1975) Calibration of the pressure dependence of the R_1 ruby fluorescence line to 195 kbar. *J. Appl. Phys., 46,* 2774-2780.

Pistorius C. W. F. T., Rapoport E., and Clark J. B. (1968) Phase diagrams of H_2O and D_2O at high pressures. *J. Phys. Chem., 48,* 5509-5514.

Postma S. (1920) Le systeme ammoniaque-eau. *Rec. Trav. Chim. Pays-Bas, 39,* 515-536.

Rollet A.-P. and Vuillard G. (1956) Sur un nouvell hydrate de l'ammoniac. *C. R. Acad. Sci., 243,* 383-386. Paris, France.

Siemons W. J. and Templeton D. H. (1954) The crystal structure of ammonium oxide. *Acta Crystallogr., 7,* 194-198.

van Kasteren P. H. G. (1973) The crystallization behavior and caloric properties of water/ammonia mixtures between 70 and 300 K. *Bull. Inst. Int. Froid, Annexe, 1973-1974,* 81-87.

Yen J. (1986) Oxygen phase diagram at high pressures. Ph.D. dissertation, University of California, Los Angeles. 45 pp.